SLIM BUCKLING-RESTRAINED STEEL PLATE SHEAR WALL AND SIMPLIFIED MODEL

Ye Lu [1,*] and Guoqiang Li [2]

[1] Doctor, Department of Structural Engineering, School of Civil Engineering
Tongji University, Shanghai, China
[2] Professor, State Key Laboratory of Disaster Reduction of Civil Engineering
Tongji University, Shanghai, China
*(Corresponding author: E-mail: luyet@tongji.edu.cn)

ABSTRACT: As a promising lateral load resisting elements in new or retrofit construction of buildings, buckling-restrained steel plate shear wall (BRSW) clamed with concrete plates had gained a great deal of attention of researchers and engineers. However, almost all of BRSWs being studied and employed are in small height-to-width ratio. Actually, in some situations, slim BRSW may be more serviceable if there do not have enough space to put wide BRSWs. Moreover, a new type BRSW was proposed in this paper. Several experimental investigations had been conducted on this BRSW, including monotonic loading tests and cyclic loading tests on four sets of specimens with different height-to-width ratio from 2:1 to 4:1, as well as comparative tests on normal steel plate shear walls. The detailing of the walls was modified to improve their energy dissipation. A simplified equivalent cross-brace model was presented and verified by finite element analyses.

Keywords: Buckling-Restrained, Steel plate shear wall, Experimental study, Simplification model

1.   INTRODUCTION

Buckling-restrained steel plate shear wall (BRSW) system is one of the most commonly used lateral-load resisting systems in high-rise buildings, consisting of a steel plate shear wall with reinforced concrete wall attached to each side by bolting (Figure 1). Zhao and Astaneh-Asl [2] proposed innovative BRSW system that in traditional system the reinforced concrete wall is in direct contact with the boundary steel columns and beams, as in innovative system, there is a gap in between. Their study showed innovative wall behaved in a more ductile manner than traditional one. Guo [3] presented ellipse hole on concrete slabs to ensure freely relative slide between steel plate and reinforced concrete slabs which can be free from being crashed and prevent the steel plate from buckling. Tsai [4] studied low yielding strength BRSW with height-to-width ratio 0.43. Berman et al. [5], Vian et al. [6], Tsai et al. [7] and Li et al. [8] found the connection of the infill panel to only the beams could reduce the force in columns and avoid damage on columns untimely.

Steel plate shear walls most widely used and studied are in small height-to-width ratio. But in some cases, there will not be enough space for a wide shear wall.   Therefore, a slim shear wall (height / width >1) might be employed. Guo et al. [9] tested three BRSWs in size of 1100×1100mm (height / width = 1) with connections to only the beams, which exhibit excellent seismic behavior. More over, many experimental studies (Tsai et al. [7], Guo et al. [9], Gao [10]) showed steel plate and concrete panels at the corner were very easily to be crushed and cracked. Therefore, a new type BRSW called I-type BRSW was presented in this paper, as shown in Figure 2. In this paper, I-type BRSW was in large height-to-width ratio. Monotonic and cyclic loading tests had been conducted to reveal their seismic behaviors. At the end of the paper, simplified model was proposed for structural design.

2.   EXPERIMENT SCHEME

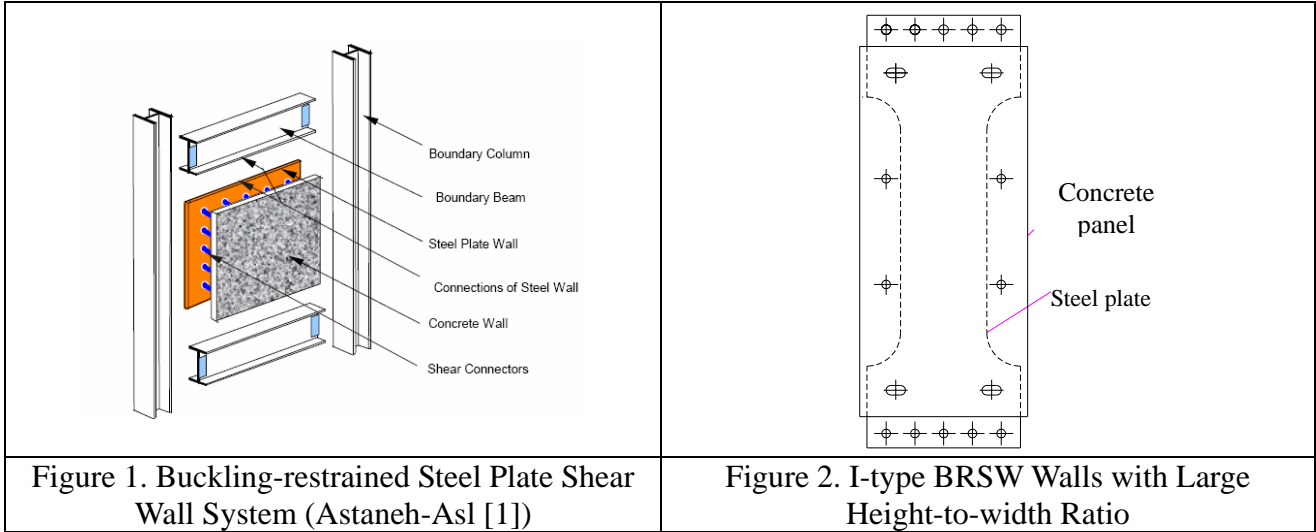|	
Figure 1. Buckling-restrained Steel Plate Shear Wall System (Astaneh-Asl [1])	Figure 2. I-type BRSW Walls with Large Height-to-width Ratio

Figure 2 showed the configuration of I-type BRSW. The steel plate had reduced section at the middle in order to improve its energy dissipating performance and protect the root from fragile damage. The steel plate was bolted or welded only to upper and lower beams. The holes on steel plate to fix concrete panels were in ellipse shape to allow free relative displacement between steel plate and concrete panels. To reveal failure mechanics, ductility performance, hysteretic behavior and ultimate load-carrying capacity of this type BRSWs, monotonic and cyclic loading tests on four sets of specimens with different Height-to-Width ratio from 2:1 to 4:1 had been conducted in Structural Lab in Tongji University.   For comparison, the tests on a set of normal SPSW specimens were also conducted.

2.1   Test Specimens

The specifications of 5 sets of specimens with 1/3-scale are shown in Table 1, and the meanings of the parameters in Table 1 are shown in Figure 3.   Each set had two segments for monotonic and cyclic loading tests respectively. Set 1 were traditional SPSWs; Set 2 to Set 5 were BRSWs.   To compare the performance of BRSWs and SPSWs, Set 4 had same size with Set 1.   Set 2 and Set 3 had same size, but the later had one more column of fixing bolts, which was used to study the influence induced by different distance between restrained bolts.

Table 1. The Specifications of Specimens

	Specimens	Description	Test Type	H (mm)	B (mm)	b (mm)	h_s (mm)	b_s (mm)	H/B	H/b	h/b
Set 1	I-180-1	Compared with Set 4	Mono	810	320	180	135	70	2.5	4.5	3
	I-180-2		Cyclic								
Set 2	IC-280A-1	BRSWs Set 3 have one more column bolts	Mono	810	440	280	125	80	1.85	3	2
	IC-280A-2		Cyclic								
Set 3	IC-280B-1		Mono	810	440	280	125	80	1.85	3	2
	IC-280B-2		Cyclic								
Set 4	IC-180-1	BRSWs Compared with Set 1	Mono	810	320	180	135	70	2.5	4.5	3
	IC-180-2		Cyclic								
Set 5	IC-140-1	BRSWs	Mono	810	300	140	125	80	2.7	5.8	4
	IC-140-2		Cyclic								

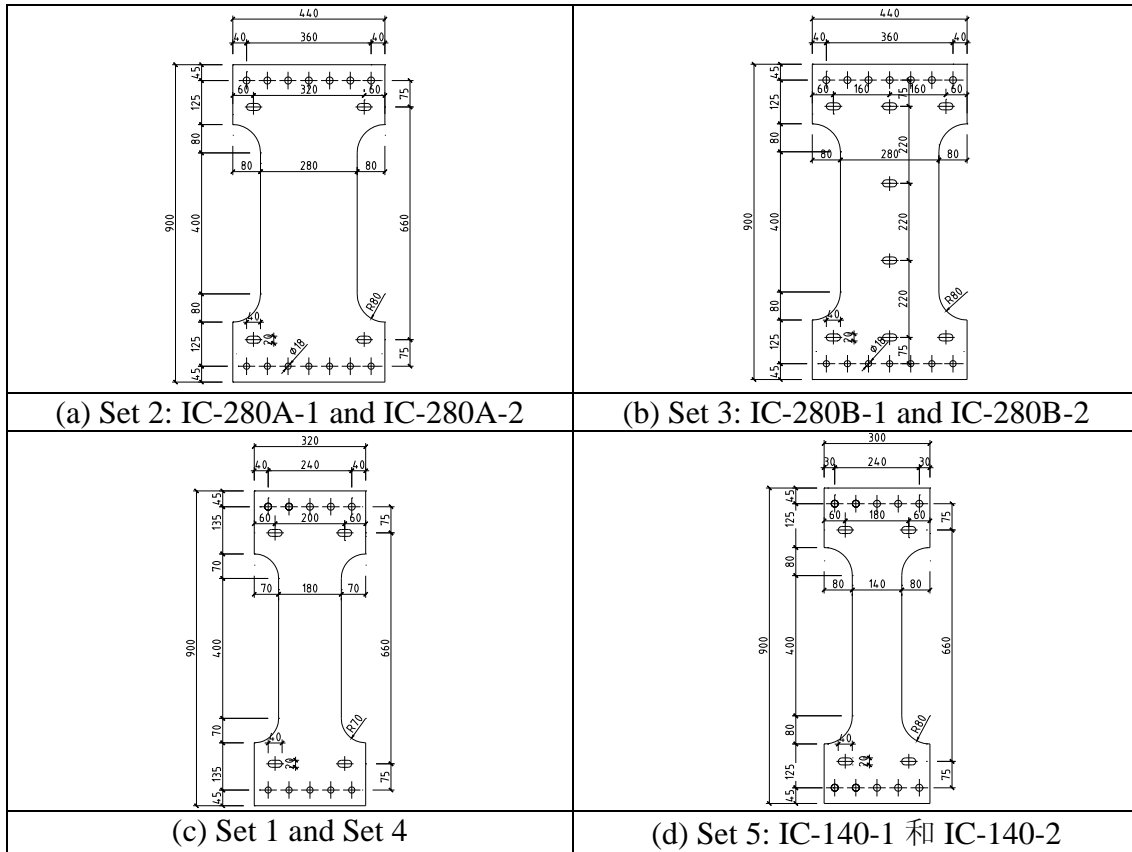| (a) Set 2: IC-280A-1 and IC-280A-2 | (b) Set 3: IC-280B-1 and IC-280B-2 |
| (c) Set 1 and Set 4 | (d) Set 5: IC-140-1 和 IC-140-2 |

Figure 3. Steel Plate of Specimens

The specimens were made of steel plate with yielding strength of about 300 MPa and thickness of 3.5mm, and two concrete panels with nominal compressive strength f_c of 28 MPa and thickness of 35mm.

2.2   Test Set-up

The diagram of test set-up was shown in Figure 4.   The beam and column were H-section with high stiffness to provide rigid boundary.   All specimens were tested on the same frame.

Lateral load and following displacements were monitored and recorded during the test (Figure 4): in-place displacement at upper end of the wall by D1 and D2 displacement gauge; slippage of bottom fish plate by D3; displacement at the base of frame by D4; out-plane displacement of frame by D5, D6 and out-plane displacement of steel plate wall by D7~D10.   Out-of-plane bracing located at the place of D5 and D6.
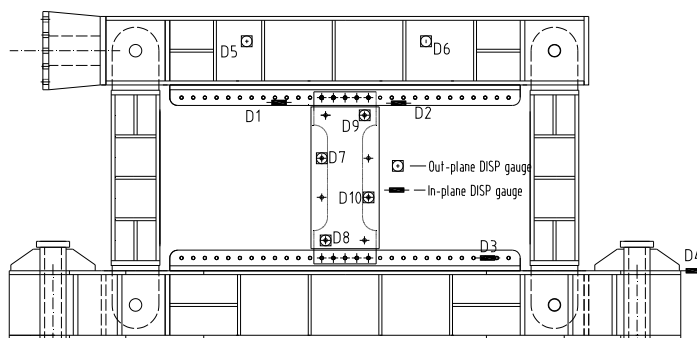

Figure 4. Test Set-up

Lateral force was applied at both end of upper beam by two single-acting jacks with maximum capacity of 20kN.   No vertical load applied on wall.   Lateral load were applied by deformation control. The maximum displacement of monotonic test was 45mm, which was about 1/20 of the height of the wall.   The yielding displacement was the essential parameter for controlling the test. The maximum lateral displacement was 25mm, which was about 1/36 of the height of the wall.

3.   BEHAVIORS OF SPECIMENS

SPSWs I-180-1 and I-180-2 buckled almost at the very early stage of test (Figure 5a). Out-of-plane deformation increased rapidly while load increased.   Buckling deformation reached to 25mm corresponding to horizontal drift of only 10mm; as horizontal drift reached 20mm, out of plane displacement was nearly 35mm.

Owing to buckling restrained by precast concrete panel, out-plane deformation of BRSWs decreased considerably.   For example, when lateral displacement reached 25mm, out-plane deformation of IC-280A-1 and IC-280B-1 is only 1mm and 2.5mm.   Even when lateral displacements reached 50mm, the maximum out-plane deformation was only 4.019mm and 4.446mm.

Due to free deformation between concrete panels and steel plate, concrete panels had kept in well status during loading without serious cracking and deformation (Figure 6a).   No fracture failure and obvious buckling occurred on steel plate (Figure 6).   However, the steel plates weren't in such a fine flat like it before test, which showed that steel plate had experienced buckling during test. It was partly due to that the precast concrete panel is too thin and small to assure required flat during manufacture.   In addition, fictional mark appeared on steel plate.

(a) Buckling at the beginning of loading   (b) Final out-plane deformation
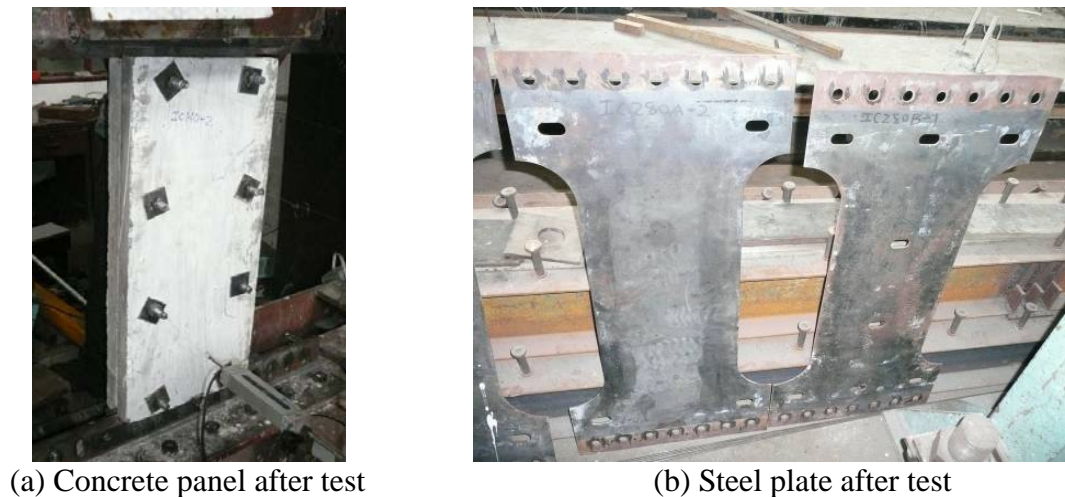
Figure 5. I-180-1 and I-180-2

(a) Concrete panel after test   (b) Steel plate after test

Figure 6. Concrete Panel and Steel Plate after Tested

4. FINITE ELEMENT ANALYSIS

Finite element analysis using ANSYS program had been conducted in order to investigate the load bearing capacity and structural performance of I-type BRSWs. Boundary frame was ignored in order not to confuse with results of the wall. The steel plate was modeled by Shell 181 (Figure 7) which is a 4-nodes element with six degrees of freedom at each node: translations in the x, y, and z directions, and rotations about the x, y, and z axes. It is well-suited for linear, large rotation analysis of thin and moderately-thick shell structures. Two methods were presented to model buckling restrained effect provided by concrete panels.

Method 1: since concrete panels did not contribute strength and stiffness to BRSW system, and they only provided restrained on out-plane deformation of steel plate, no concrete elements were modeled in FE models. The buckling restrained function of concrete panels was simulated by simply defining out-plane deformation of steel plate as 0 (Figure 8).

Method 2: concrete panels were modeled by solid 65 and the nodes on the concrete panels were coupled with inner steel plate in the out-of-plane direction (z direction), at the positions with bolts.

Two methods were used to analyze the specimen IC-180-1 respectively. Comparison of Force-Displacement curves with test results (Figure 9) showed method 1 has better accurateness than method 2. Moreover, it was simpler. Therefore, in FE analysis, method 1 was adopted to simulate the function of concrete panels.

The lateral force acted at the top of plate. The bottom end of steel plate was fixed in 6 degrees of freedom. The up end of steel plate was fixed in 5 degrees of freedom. The X degree was free, but the nodes at up end edge were coupled with the node on which the force acted. The first elastic buckling mode was adopted as the imperfection shape of steel plate. Figure 10 showed stress distribution after yielding of the steel plate.
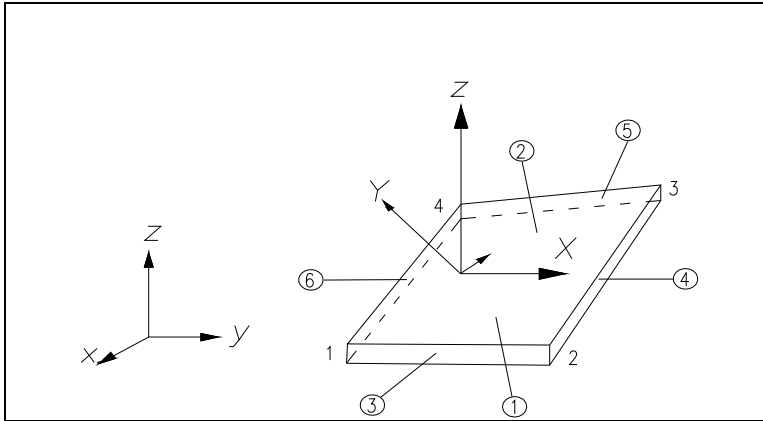
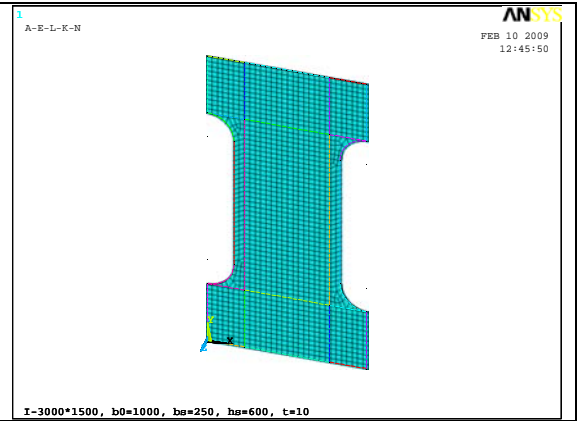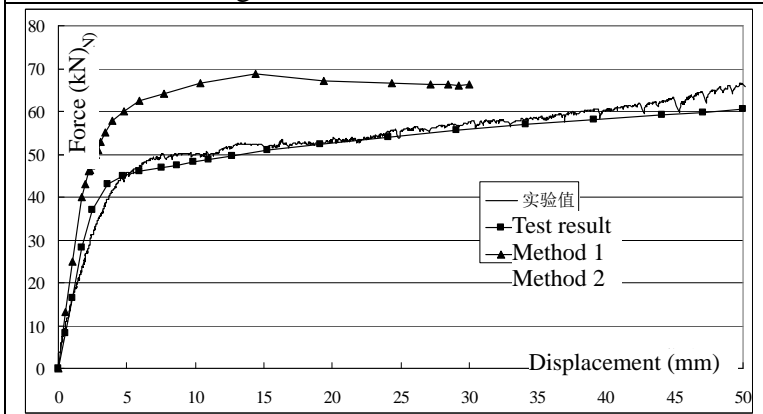Figure 7. Shell 181 Element

Figure 8. FE Element

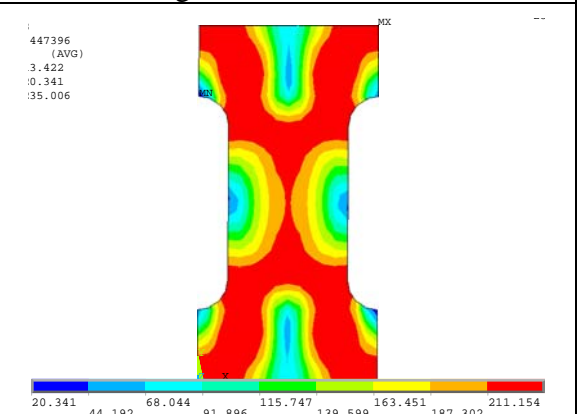Figure 9. Comparison of Force-Displacement Curves

Figure 10. Stress Distribution after Yielding of the Steel Plate

5.   ANALYSIS ON TEST RESULTS

5.1   Monotonic Test

Monotonic curves of all specimens are shown in Figure 7 and Table 2, compared with finite element curves obtained from ANSYS. Results obtained from test and FE analyses were coincident quite well, except of IC-140-1 in plastic range. The reason was that the concrete panels touched fish plate and increased loading capacity.
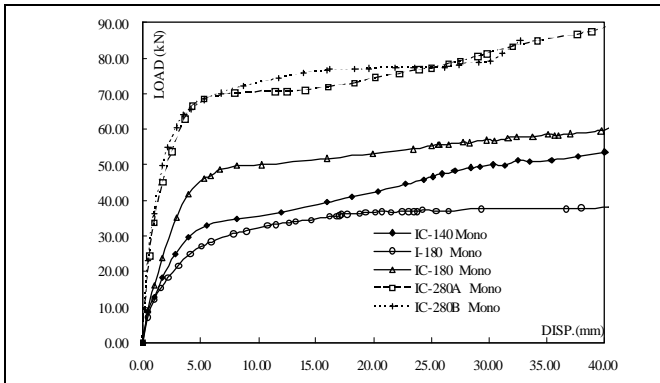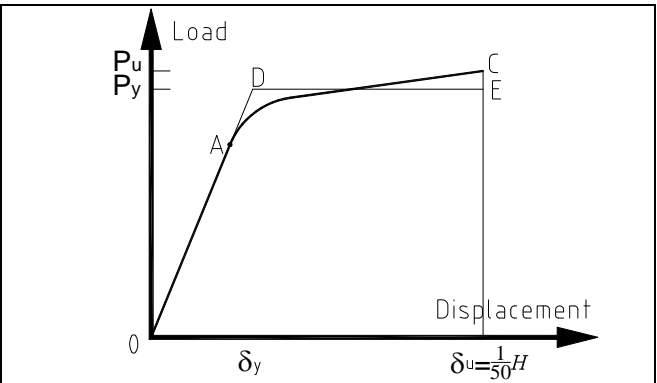

Figure 7. Monotonic Curves of All Specimens

Figure 8. Determination of Yielding Point

Yielding points were determined by Energy-Equal Protocol as shown in Figure 8. Ultimate displacement δ_u was defined as 1/50 of wall height, i.e. 16.2mm. Ultimate loading point C was determined by δ_u. Prolong initial elastic curve OA to point D. Horizontal line DE crossed line Cδ_u at Point E. According to Energy-Equal Protocol, the area enclosed by OAC and X-axis should be equal to that enclosed by ODE and X-axis. Therefore, Point D can be determined, and it indicated nominal yielding strength P_y and yielding displacement δ_y. Ductility coefficient μ was the ratio between δ_u and δ_y.

Table 2. Parameters Comparison of Specimens

		Initial stiffness (kN/mm)	Nominal yielding point P_y(kN)	Yielding displacement δ_y(mm)	Ultimate strength P_u(kN)	Ductility coefficient
Set 1 I-180	FE analysis	11.06	29.92	2.71	32.94	5.98
	Test result	14.24	29.69	2.08	35.68	7.79
Set 2 IC-280A	FE analysis	32.80	72.85	2.22	78.39	7.30
	Test result	40.8	66.91	1.64	72.09	9.88
Set 3 IC-280B	FE analysis	32.80	72.85	2.22	78.39	7.30
	Test result	32.45	70.88	1.51	76.58	10.73
Set 4 IC-180	FE analysis	15.50	49.09	3.17	52.33	5.11
	Test result	20.80	46.61	2.24	51.92	7.23
Set 5 IC-140	FE analysis	10.77	27.94	2.59	30.56	6.25
	Test result	16.67	33.24	1.99	39.34	8.14

Compared Set 1 and Set 4, ultimate strength, yielding point and initial stiffness of the later increased obviously due to buckling restrained contributed by concrete panel.

The distance between restrained bolts would affect restrained effect from concrete panel, which can not be derived from FE analysis accurately. Compared Set 2 and Set 3, in plastic range, the curve of IC-280A-1 descended a little bit, which demonstrated slight buckling on steel plate. However, the buckling didn't develop too much. Yielding strength and ultimate strength of IC-280B-1 is greater than IC-280A-1, but not too much. Generally, the load versus displacement curves of specimens was similar to FE results.

Owing to the contribution of concrete panel, initial stiffness and ultimate strength obtained by test were higher than FE analysis.

5.2 Cyclic Loading Test

Cyclic loading curves are shown in Figure 9 and in well symmetric. The hysteresis curve of I-180-2 pinched seriously due to buckling (Figure 9a), which reflected bad energy dissipating performance. Compared with SPSW, the hysteresis curves of BRSWs were fairly wide (Figure 9 b, c, d), indicating good energy dissipating. However, after lateral displacement reached to 10mm, the curve of IC280-2 and IC180-2 appeared long yielding platform. Slight buckling of steel plate might be one of possible reasons. Meanwhile, during the course of test, the slippage of bolting connection of steel plate and beam, which exerted obvious sound, could reduce load bearing capacity. However, BRSWs still displayed good energy dissipating performance. In Figure 9c, IC280B-2 which had one more column of bolts showed higher load bearing capacity than IC280A-2, but the difference wasn't so much great.

(a)   I-180-2

(b) IC-280A-2 and IC-280B-2
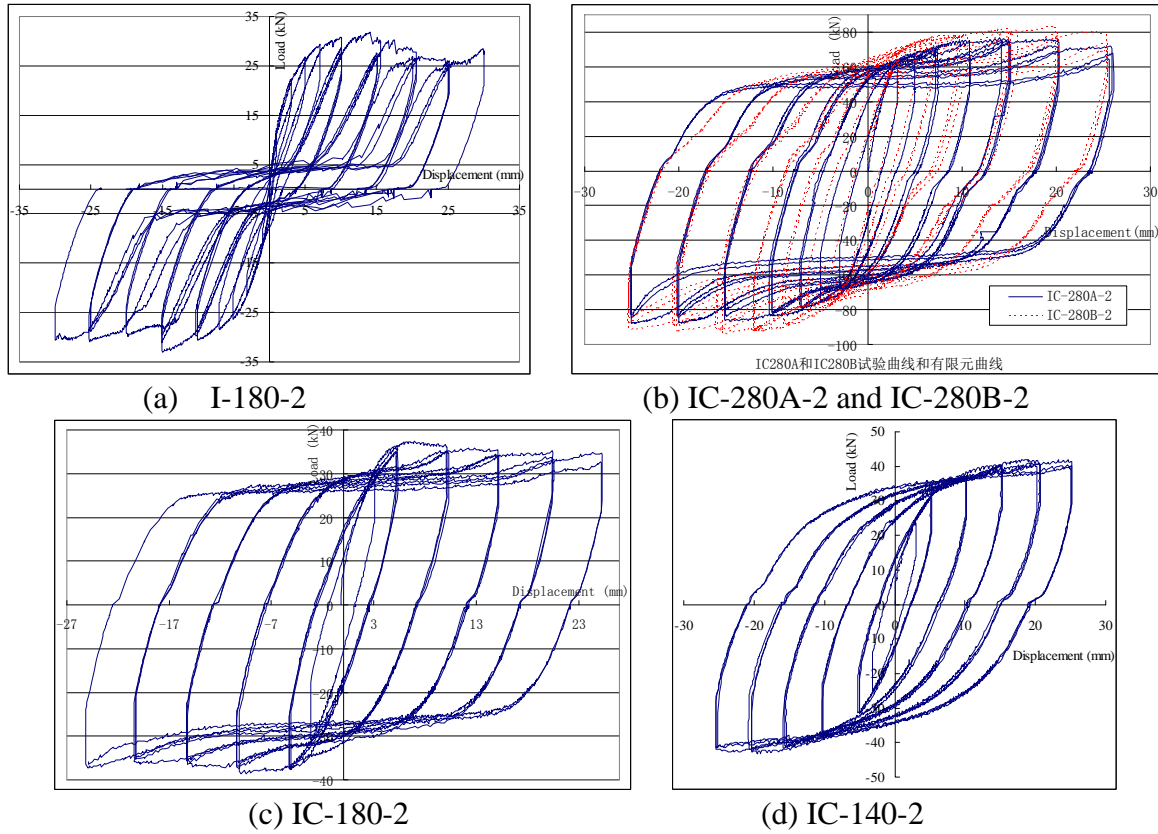
(c) IC-180-2

(d) IC-140-2

Figure 9. Cyclic Curves of All Specimens

In Figure 9d, the hysteresis curve of IC-140-2 was quite wide and there was no pinch and no yielding platform.
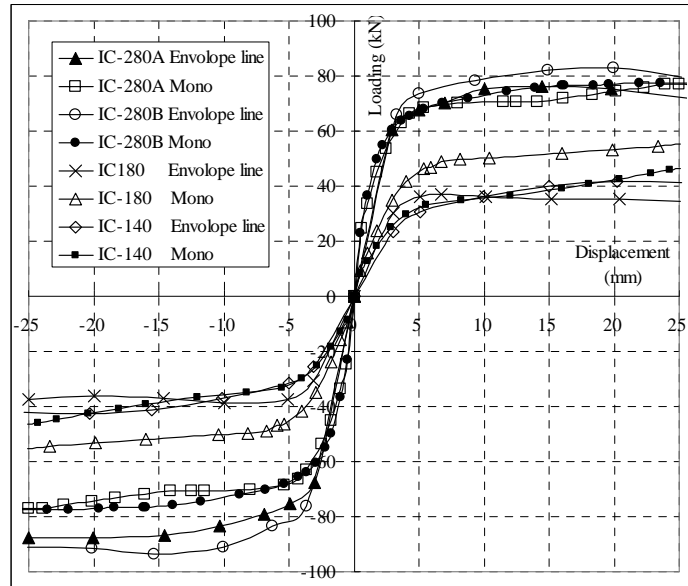

Figure 10. Comparison of Envelope Lines of Cyclic Loading and Monotonic Test Curves

Figure 10 showed comparison of envelope lines of cyclic loading and monotonic test curves respectively.   All of the walls had stable load bearing capacity without abrupt increasing or decreasing.   Except of IC180, envelope lines of cyclic test were quite close to that of monotonic test.   Load bearing capacity in cyclic test of IC-180-2 was much less than that in monotonic test and even approached to the curves of IC140.   Two reasons could explain this: 1) buckling

occurred in the test of IC-180-2 due to rough surface of concrete panel; 2) IC-180-2 was the last one to be tested, and the fish plate became very slippery because of friction by former tests. The slippage of base bolt was very serious, which decrease the load bearing capacity.

6. SIMPLIFIED MODEL

For convenience in engineer's application, some simplified models of steel plate shear walls were proposed before. Most of them were strip models, which were reasonable for the infill panel connected both to beams and columns, or a wide wall. For slim and two sides connecting I-type BRSWs studied in this paper, strip models were not appropriate.

Zhang [11] adopted equivalent braces to represent the slit RC shear wall based on an equivalent lateral stiffness. Numerical results indicated that equivalent braces could be effectively utilized for the global static analyses of frame structures. Wang [12] applied equivalent eccentric cross braces model to simulate steel plate shear wall with vertical slits and received similar force and deformation of the structures.

Therefore, this paper adopted equivalent eccentric cross braces to simulate slim I-type BRSW. The principle was shown in Figure 11a. Since the steel plate was buckling restrained, it could bear pressure. Therefore, the simplified braces could bear tension and pressure. After critical parameters, such as cross sectional area, load bearing capacity of equivalent cross braces, as well as the eccentric distance e of the braces from the edge of BRSWs, were determined, engineers can build up design models in normal structural design software and get the internal forces of frame members.

Cross sectional area of brace can be determined by initial stiffness of BRSWs according to stiffness equivalent principle. According to Figure 11b, as lateral force F acting on the frame, the lateral drift Δ_w will be:

$$\Delta_w = \frac{\Delta_b}{\cos\beta} = \frac{Fl_b}{2EA_b\cos^2\beta} \tag{1}$$

Where A_b = the cross sectional area of brace; E = elasticity modulus; Δ_b, β, l_b, are shown in Figure 11b.
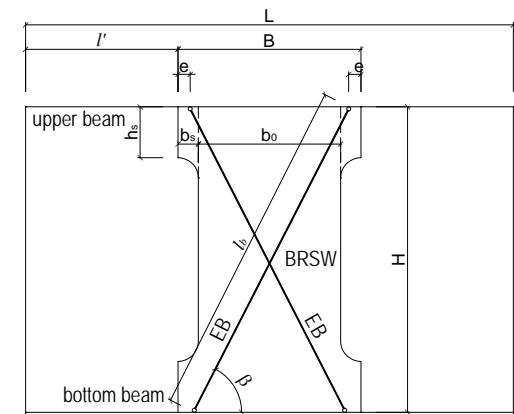
(a) Principle of Equivalent Eccentric Cross Braces Model
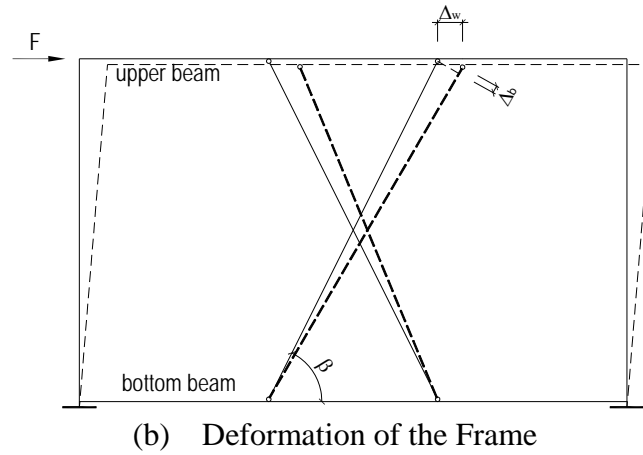
(b)   Deformation of the Frame

Figure 11. Equivalent Eccentric Cross Braces Model

With the stiffness equivalent principle, we have $F=K\times\Delta_w$

Therefore, the cross sectional area of brace A_b should be:

$$A_b = \frac{Kl_b}{2E\cos^2\beta}$$ (2)

Where K= initial stiffness of BRSWs. K could be determined by finite element analyses, or according to Lu. Y. [13], for I-type BRSWs, initial stiffness of BRSWs K could be derived by following formula:

$$K = \frac{1}{\Delta} = \frac{1}{\zeta+\delta} = \frac{G\times t\times b'_0}{H} + 12\frac{EI}{H^3} = \frac{Et}{2.6\frac{H}{\beta b_0} + (\frac{H}{\beta b_0})^3}$$ (3)

Where G = shear modulus of the steel plate, $G=E/2(1+\upsilon)=\dfrac{E}{2.6}$; υ = poison ratio of the steel plate; H, t = respectively, the height, thickness of the steel plate; I = inertia moment of the cross section of the steel plate.

β was a parameter which has a relationship with the enlarged area of the end. According to large quantities analyses, β can be written in:

$$\beta = \frac{A+A_s}{0.95A} = 1.053 + \frac{4(h_s+b_s)b_s - \pi b_s^2}{Hb_0}$$ (4)

Where, $A = H\times b_0$; $A_s= 4\times(h_s+b_s)\times b_s-\pi b_s^2$, the enlarged area at the end of plate; h_s, b_s= enlarged dimension of the end, seen Figure 12b.
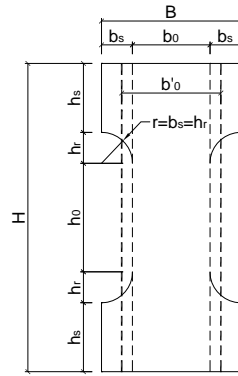
Figure 12. Revising of the Width for I-type Walls

To find the eccentric distance e, massive finite element analyses of BRSWs with various sizes had been conducted. The influences on e under different parameters had been studied, including width B, clear width b_0, height H, enlarged size b_s and h_s, distance to column l', which indicated the location of the BRSW in the frame, as well as different connections of beams and columns, i.e. moment or simple connection. Numerical analysis showed the eccentric distance e only has relation with width B and l'. Therefore, empirical formula was supposed as:

$$\begin{cases} e = 50mm, (l' \geq 700mm) \\ e = (2.93 \times 10^{-4} \times B - 0.1969)l' + 0.015B + 25, (l' > 700mm) \end{cases} \tag{5}$$

Table 3 showed the comparison of frame drift and maximum moment in beams between BRSWs and EB frames. The BRSWs located at the middle of frame. The beam section is H150×250×10×16, and the column section is H250×250×16×16. Length of beam L= 4800mm, height of column and BRSWs H=3000mm, thickness of BRSWs = 10mm, h_s=600mm, b_s=200mm. The clear width of wall b_0 was various, and two kinds of connections of column to beam were considered, one was moment connection and the other was simple connection. Figure 13 demonstrated the distribution of moment in upper beam between original and simplified frames. Results showed the maximum moment in frames and frame drifts were very similar, both for two kinds of frames. However, as the height-to-width ratio of BRSWs decreased (the wall became wider), the moment curve displayed depressing phenomenon in the range of walls, which was due to that wide BRSWs could bear shear force with the beam. Although equivalent cross braces could not simulate this phenomenon, structural design are usually determined by maximum value of forces in structural members that the simplified model could have enough accurateness. Table 3 also showed b_0 had no influence on the value of eccentric distance e. Additionally, analyses also showed the maximum value of moments in the beams of simple connection frames were larger than that in moment frames. However, if the walls were put continuously vertically, the moments in a beam caused by upper and lower BRSWs could counteract to each other. Only the top and bottom beams need special attention.

Table 3. Comparison of Drift and Moment between BRSWs and EB Frame

Frame	Connection of column to beam	b_0 (mm)	BRSWs frame		e (mm)	EB frame		Error on moment	Error on drift
			Maximum moment in beams (kN·m)	Drift (mm)		Maximum moment in beams (kN·m)	Drift (mm)		
S-b0-600-M	moment	600	43.54	8.15	50	46.46	7.48	6.71	-8.22
S-b0-1200-M	moment	1200	43.83	5.48	50	42.5	5.41	-3.03	-1.28
S-b0-1800-M	moment	1800	36.38	3.74	50	35.95	3.83	-1.18	2.41

Frame	Connection of column to beam	b_0 (mm)	BRSWs frame		e (mm)	EB frame		Error on moment	Error on drift
			Maximum moment in beams (kN·m)	Drift (mm)		Maximum moment in beams (kN·m)	Drift (mm)		
S-b0-2400-M	moment	2400	27.00	2.39	50	27.81	2.56	3.00	7.11
S-b0-600-J	simple	600	138.78	31.91	50	150.40	28.79	8.37	-9.78
S-b0-1200-J	simple	1200	143.05	21.72	50	146.63	21.34	2.50	-1.75
S-b0-1800-J	simple	1800	129.87	14.95	50	132.32	15.47	1.89	3.48
S-b0-2400-J	simple	2400	109.31	9.32	50	111.33	10.47	1.85	12.34
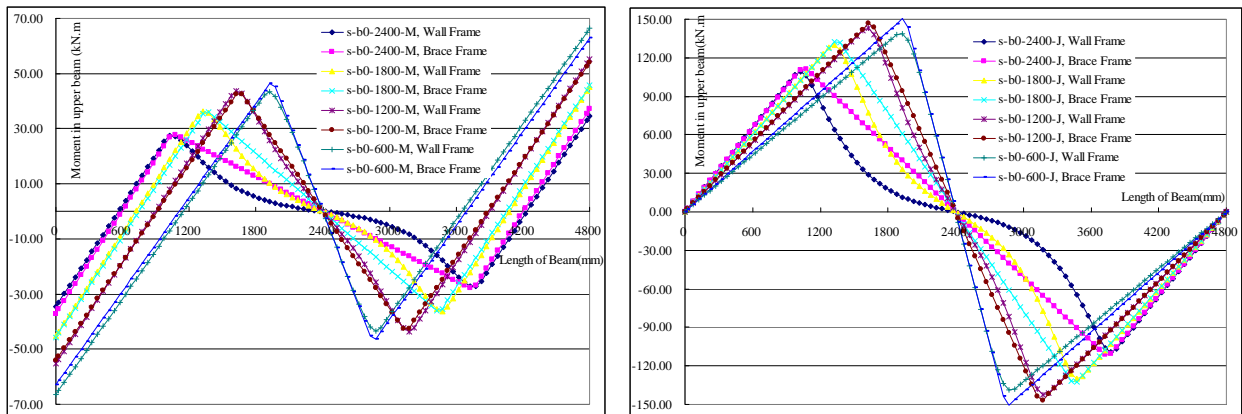
(a) Moment comparison in moment frames   (b) Moment comparison in simple connection frames

Figure 13. Comparison of Moment in Upper Beam between Frames with BRSWs and EB

7.   CONCLUSION

The following concluding remarks may be drawn through this research:

1) Compared with normal steel plate shear walls, BRSW walls have stable and wide hysteresis curve, exhibiting good plastic deformation ability, and energy dissipating performance;

2) The growing circle bore to fix concrete panel could allow free deformation of steel plate during the course of loading and keep the concrete panel in sound condition.   Therefore the concrete wall can have good performance as buckling restrained panel.

3) Bolting connector at the base of steel plate wall with beam is apt to slip, which could decrease load bearing capacity;

4) BRSW walls exhibited good mechanics performance, and no fracture failure occurred at the end of steel plate;

5) Simplified cross brace model were very convenient and had acceptable accurateness for the structural design of frame with BRSWs.

ACKNOWLEDGEMENT

REFERENCES

[1]   Astaneh-Asl, A., "Seismic Behavior and Design of Composite Steel Plate Shear Walls", Steel TIPS Report, Structural Steel Educational Council, Moraga, Calif, 2002.

[2]   Zhao, Q.H. and Astaneh-Asl, A., "Cyclic Behavior of Traditional and Innovative Composite Shear Walls", Journal of Structural Engineering, ASCE, 2004, Vol. 130, No.2, pp. 271-285.

[3]   Guo, Y.L. and Dong Q.L., "Static Behavior of Buckling-Restrained Steel Plate Shear Walls", Tall Buildings from Engineering to Sustainability, ED: Cheung Y.K., Chau K.W., 2005, pp. 666-670.

[4]   Tsai, K.C., Lin, Y.C. and Lin, C.H., "Seismic Responses and Design of Steel Plate Shear Wall", Proceedings of The Fourth Cross Strait & Hong Kong Conference on Steel Structures, Shanghai, China, 2006, pp. 108-116. (in Chinese)

[5]   Berman, J. and Bruneau, M. "Plastic Analyses and Design of the Steel Plate Shear Walls", Journal of Structural Engineering, 2003, Vol. 129, No.11, pp. 1448-1456.

[6]   Vian, D. and Bruneau, M. "Steel Plate Shear Walls for Seismic Design and Retrofit of Building Structure", Technical Report MCEER-05-0010, Multidisciplinary Center for Earthquake Engineering Research, Buffalo, New York, 2005.

[7]   Tsai, K.C., Lin, C.H., Lin, Y.C., Hsieh, W.D and Qu, B. "Sub-structural Hybrid Tests of A Full Scale 2-story Steel Plate Shear Wall", Technical Report NCREE-06-017, National Center for Research on Earthquake Engineering, Taipei, Taiwan, 2006.

[8]   Li, C.H., Tsai, K.C. and Lin, C.H., "Cyclic Tests of Four Two-story Narrow Steel Plate Shear Walls", The Proceedings of the 5th International Symposium on Steel Structures, March 12-14, Seoul, Korea, 2009, pp. 237-245.

[9]   Guo, L.H., Ma, X.B., Zhang, S.M. and Guan N., "Experimental and Theoretical Analyses of Composite Shear Walls with Two-Side Connections", The Proceedings of the 5th International Symposium on Steel Structures, March 12-14, Seoul, Korea, 2009, pp. 710-716.

[10]   Gao, H., "Experimental and Theoretical Studies on Composite Steel Plate Shear Walls" (in Chinese), Dissertation submitted to Tongji University in Conformity with the Requirements for the Degree of Master, 2007.

[11]   Zhang, Y.C., Liu, Y.H., etc., "A Simplified Model for Static Analyses of Slit RC Shear Walls", China Civil Engineering Journal, 2006, Vol. 39, No. 9, pp. 62-68.

[12]   Wang, W.T., "Experimental and Theoretical Study on Buckling Restrained Steel Plate Shear Wall with Slits", Dissertation submitted to Tongji University in Conformity with the Requirements for the Degree of Master, 2008.

[13]   Lu, Y., "Research on the Steel Frame of Bound-Column System with Buckling Restrained Steel Plate Shear Wall in Large Aspect Ratio", Dissertation submitted to Tongji University in Conformity with the Requirements for the Degree of PHD, 2009.

RANDOM EQUIVALENT INITIAL BOW AND TILT
IN STEEL FRAME

A. Machowski [1] and I. Tylek [2, *]

[1] *Assoc. Prof. D. Sc. Ph. D., Faculty of Civil Engineering,*
Cracow University of Technology, ul. Warszawska 24, 31-155 Cracow, Poland,
[2] *Assist. Prof. Ph. D., Faculty of Civil Engineering,*
Cracow University of Technology, ul. Warszawska 24, 31-155 Cracow, Poland
*(Corresponding author: E-mail: ik2@poczta.fm)

ABSTRACT: Probabilistic models of equivalent geometrical imperfections suitable to analysis of steel buildings frames are under consideration. Statistically based models of equivalent imperfections, besides of application in structural reliability analysis, should be taken as basis of verification of equivalent imperfection formulas and rules of introducing imperfections into frame calculations proposed in different Standards. Column random equivalent initial bow was obtained in this paper utilizing randomization of buckling coefficient in well-known deterministic formula of equivalent initial bow. Problem of random equivalent initial tilt of frame was considered for spatial mechanical model of skeletal structure, braced by rigid floor disks, using results of existing buildings geodesic measurements statistical analysis. In the paper assessment of random initial tilts and initial bows joint effect is commented.

Keywords: Multistory steel frame, Random equivalent geometrical imperfection, Eurocode 3

1.   INTRODUCTION

Carrying capacity of steel frames significantly depends on imperfections (Table 1(a)): single column; residual stresses and axes misalignments as well as bar system imperfections; column out-of-plumbs, eccentricity in column field joints, assembly stresses, random joint rigidity.

In traditional approach (Chen and Toma [1], Narayanan [2]) imperfections are modeled by linear combination of buckling modes (simplifying – only dominant buckling mode) which correspond to solution of bifurcation problem using linearized model of perfect system elastic stability. In this approach real structure imperfections are taking into consideration only indirectly – by using standard buckling curves. Column out-of-plumbs and other important imperfections, arising during assembly, are passed over in traditional approach.

Contemporary standard approach depends on taking into account of two equivalent geometrical imperfections (Table 1(b)): equivalent initial column bow e_0 (column misalignment and column residual stresses) and equivalent initial frame tilt ϕ_0 (column out-of-plumbs, eccentricity in column field joints, assembly stresses, randomness of beam-column joints rigidity).

Standard approach approximately takes into consideration steel skeleton fabrication conditions, in particular (Figure 1): columns division on assembly parts and its assembly with random out-of-plumbs – causing significant changes of moment values in equilibrium equations – because of large vertical forces occurrence.

Table 1. Conceptions of Equivalent Geometric Imperfections

(a) Imperfections of compressed bar and frame				
compressed bar		frame		
residual stresses	misalingment	column out-of-plumb	joints eccentricity	joints stiffness randomness

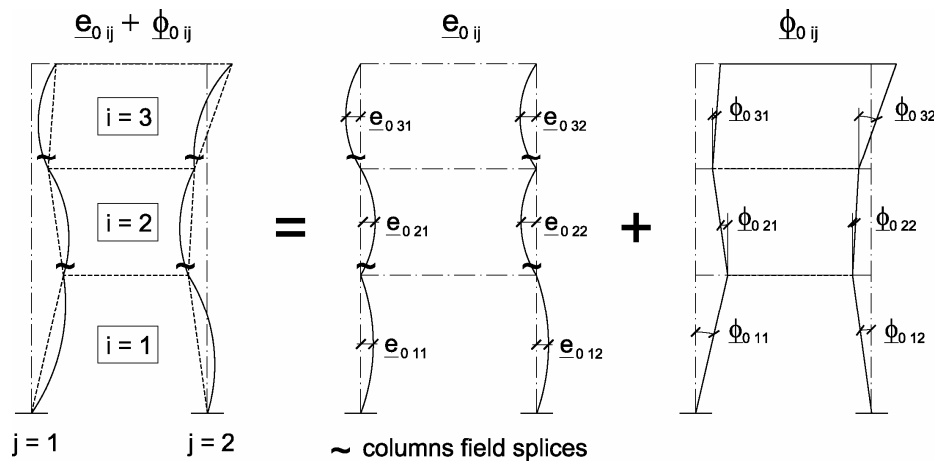| (b) Equivalent geometric imperfections	
compressed bar	frame
equivalent initial bow	equivalent initial tilt (equivalent initial sway ratio)

Figure 1. Columns Random Initial Bows and Initial Tilts

Issues connected with research and modeling of equivalent geometrical imperfections e_0 and ϕ_0 are discussed in chapters 2 to 4 of this paper.

2.   RANDOM EQUIVALENT INITIAL BOW OF COLUMN

Random equivalent initial bow of column is obtained as function of random buckling coefficient $\underline{\varphi}$ (random values are underlined).

Random buckling coefficient was determined in papers (Machowski, A. [3]) utilizing Fukumoto and Itoh statistical data (Fukumoto, Y. and Itoh, Y. [4]) and applying randomization of axially compressed steel bar flexural buckling resistance standard formula

$$\underline{N}_{b.R} = \underline{\varphi} \cdot \underline{N}_{pl} \, . \tag{1}$$

It was assumed that random flexural buckling resistance of compressed steel bar $\underline{N}_{b.R}$ and bar cross-section random plastic resistance $\underline{N}_{pl}$ have logarithmic-normal distribution[(*)] – stable (invariant) with respect to multiplication and defined only for positive values of $\underline{N}_{b.R}$ and $\underline{N}_{pl}$.

It follows that stochastically independent (originally) from $\underline{N}_{pl}$ buckling coefficient φ has also logarithmic-normal distribution. Flexural buckling resistance $\underline{N}_{b.R}$ has median equal to product of medians $\breve{N}_{b.R} = \breve{\varphi} \cdot \breve{N}_{pl}$ and logarithmic coefficient of variation equal to vector sum of logarithmic coefficients of variation $v_{Nb.R} = \sqrt{v_{\varphi}^2 + v_{Npl}^2}$.

Appropriate sets of data have been statistically processed with a mean-square approximation of experimental values of medians $\breve{\varphi}(\Lambda)$ and logarithmic coefficients of variation $\breve{v}_{\varphi}(\Lambda)$, where $\Lambda = \sqrt{\breve{N}_{pl} / \breve{N}_E}$ - relative slenderness ($\breve{N}_E$ - median of bar Euler's resistance) and application of formulas:

$$\breve{\varphi}(\Lambda) = (1 + \Lambda^{2n})^{-\frac{1}{n}}, \qquad \breve{v}_{\varphi}(\Lambda) = v_m \cdot \left(\frac{2 \cdot l \cdot \Lambda}{1 + (l \cdot \Lambda)^2} \right)^2 . \tag{2}$$

Empirical parameters (Machowski, A. [3]): n, v_m, and l for buckling curves: "a", "b" and "c" (CEN [5], PKNMiJ [6]) are presented in Table 2.

Table 2. Empirical parameters for formula (2)

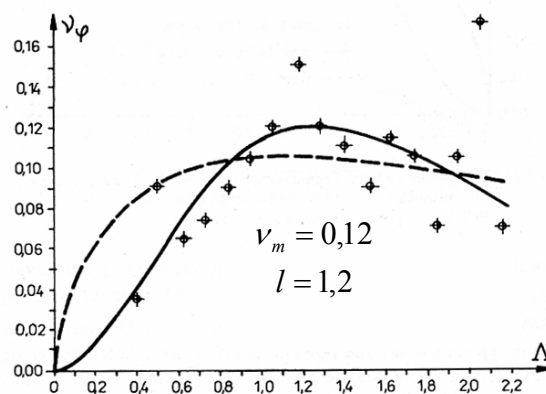|	Buckling curve		
	a	b	c
n	3,0	2,6	2,2
v_m	0,10	0,11	0,13
l	0,8	0,9	1,0

Figure 2. The Example of Values $v_{\varphi}(\Lambda)$ Approximation for $N = 1251$
Column Research Council Test Results (Machowski [3])

[(*)]   parameters   of   logarithmic-normal   variable $\underline{X} > 0$ with   probability   density   function $f(x) = \frac{1}{\sqrt{2\pi} \cdot v_X \cdot X} \cdot \exp(-\ln^2(X / \breve{X}) / (2 \cdot v_X^2))$; mean value $\overline{X} = E\{X\}$ and coefficient of variation v_X are related as follows: $\breve{X} = \overline{X} / \sqrt{1 + v_X^2}$, $v_X = \sqrt{\ln(1 + v_X^2)}$.

An example of experimental coefficients of variation approximation by means of function $v_\varphi(\Lambda)$ according to Eq. 2 is shown in Figure 2; single points represent empirical mean values of $v_\varphi^*(\Lambda)$ connected with individual slenderness Λ. Form of function (2) refers to earlier proposals connected with stability coefficients (PKNMiJ [6], Allen [7], Rondal and Maquoi [8]).

For logarithmic-normal distribution parameters: $\breve{\varphi}$, v_φ and design value φ_d of buckling coefficient $\underline{\varphi}$ are related as follows

$$\varphi_d \stackrel{df}{=} N_{b.Rd} / N_{pl,d} = \breve{N}_{b.R} \cdot \exp(-\beta_R \cdot \sqrt{v_\varphi^2 + v_R^2}) / (\breve{N}_{pl} \cdot \exp(-\beta_R \cdot v_R)) =$$
$$= \breve{\varphi} \cdot \exp(\beta_R \cdot (v_R - \sqrt{v_\varphi^2 + v_R^2})). \tag{3}$$

Introducing into Eq. 3 values according formula (2) and Table 2, $v_R = 0,10$ (according to (Murzewski [9])) for random plastic resistance of steel $\underline{R} \equiv \underline{f}$ ($\underline{R} = \underline{N}_{pl} / \underline{A}$) corrected for random deviation of bar cross-section area $\underline{A}$ and partial reliability index $\beta_R = 3,0$ relationship $\varphi_d(\Lambda)$ was received. This relationship was compared (for buckling curve "b") in Figure 3 with other curves characterizing buckling coefficient.
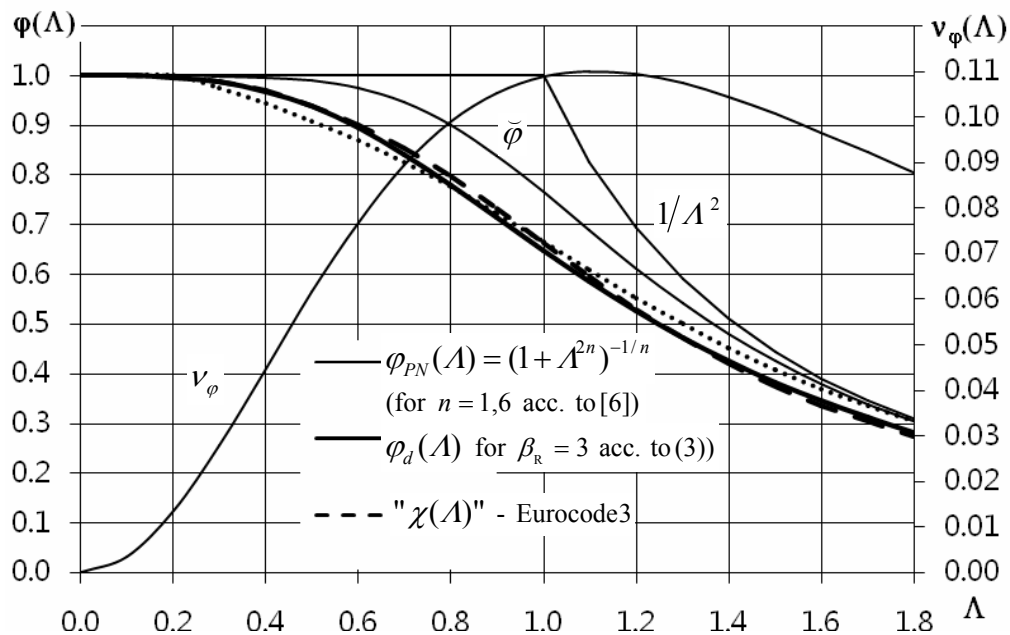

Figure 3. Parameters $\breve{\varphi}$ and v_φ and Different Relationships $\varphi_d(\Lambda)$ for Buckling Curve "b"

Design values of φ_d obtained from Eq. 3 for $\beta_R = 3,0$ and parameters according to Table 2 are very close to standard values of $\varphi_{PN}(\Lambda)$ from Polish Standard [6] and values of $\chi(\Lambda)$ from Eurocode [5] (it was shown in Figure 3 – for buckling curve "b") if following relationship will be used

$$\Lambda = 1,1178 \cdot \overline{\lambda} \cong 1,12 \cdot \overline{\lambda}. \tag{4}$$

Relationship (4) may be obtained by assuming in general formula for relative slenderness

$$\lambda_r \stackrel{df}{=} \sqrt{N_{pl} / N_E} \cong \lambda / (\pi \cdot \sqrt{E / R_{pl}}) = \lambda / \lambda_1, \tag{5}$$

medians: $E = \breve{E} = 205$ GPa and $R_{pl} = \breve{f} = 290$ MPa (hence $\lambda_1^{PN} = 84$) – as it was made in Polish Standard [6] for low-carbon steel or values: $E = 210$ GPa and $R_{pl} = f_y = 235$ MPa (hence $\lambda_1^{EC} = 93,9$) – according to Eurocode [5].

To determinate column random equivalent initial bow we use well-known formula of dimensionless equivalent initial deflection ε_0 (Rondal And Maquoi [8], ECCS [10]) of hinged bar with sinusoidal initial bow (the formula is based on bar resistance conservation criterion)

$$\varepsilon_{0e} = e_{0e}/r = (\varphi^{-1} - 1) \cdot (1 - \varphi \cdot \Lambda^2) = \varphi^{-1} + \varphi \cdot \Lambda^2 - (1 + \Lambda^2),$$ (6)

where: e_{0e} - bar equivalent initial bow,

$r \equiv W/A$ - radius of cross-section core.

Random imperfection $\underline{\varepsilon}_{0e} = \underline{e}_{0e}/r$ is obtained utilizing randomization of Eq. 6 by introducing in place of φ random bucking coefficient $\underline{\varphi}$ with logarithmic-normal distribution and parameters according to formulas (2) and Table 2. It follows that we have to determinate $\underline{\varepsilon}_{0e}$ probability distribution as a known deterministic function $\varepsilon_{0e}(\underline{\varphi})$ of the known random variable $\underline{\varphi}$.

According to mechanical interpretation and property of logarithmic-normal distribution quantity $\varepsilon_{0e} = e_{0e}/r$, similarly as other quantities in Eq. 6, are treated as non-negative (or positive) what follows that function $\varepsilon_{0e}(\varphi)$ is determined for $\varphi \in (0, \min(1, 1/\Lambda^2)]$. In this range of φ values function $\varepsilon_{0e}(\varphi)$ is monotonically decreasing (Figure 4(a)) and probability density function $g(\varepsilon_{0e})$ amounts to transformation type (Papoulis [11]):

$$g(y) = f(u^{-1}(y)) \cdot \left| \frac{du^{-1}(y)}{dy} \right|$$ (7)

where: $f(x)$ - known probability density function of random variable $\underline{x}$,

$u^{-1}(y_x)$ - inverse function of given function $y = u(x)$ - strictly monotonic,

$g(y)$ - inquired probability density function of random variable $y = u(\underline{x})$.

Logarithmic-normal distribution, rational in case of coefficient φ (definite for $\varphi > 0$ and stable in relation to multiplication) does not fulfil yet condition $\varphi \leq \varphi_{max} = \min(1, 1/\Lambda^2)$. To calculate density function $g(\varepsilon_{0e})$ we introduce corrected (cut off) distribution $\underline{\varphi}$ with density $c \cdot f(\varphi)$, where: $c = 1/(1 - \omega_m)$ - normalizing factor, $\omega_m = \text{Prob.}\{\varphi \geq \varphi_{max}\}$ (Figure 4(a)). This adoption we propose for skeleton column slenderness $\Lambda \leq \sim 1,4$ (that is $\lambda < \sim 120$). For slenderness values distant from 1 coefficient c increases significantly.

After introducing into Eq. 7 function $\varepsilon_{0e}(\varphi; \Lambda)$ and corrected logarithmic-normal probability density function $f(\varphi; \Lambda)$ with parameters $\varphi(\Lambda)$ and $v_\varphi(\Lambda)$ we obtain density function of random variable $\underline{\varepsilon}_{0e}$ in the form of:

$$g(\varepsilon_{0e};\Lambda)=\frac{c}{\sqrt{2\pi}\cdot v_\varphi\cdot\varphi(\varepsilon_{0e})}\cdot\exp\left\{-\frac{\ln^2\left(\varphi(\varepsilon_{0e})/\breve{\varphi}\right)}{2\cdot v_\varphi^2}\right\}\cdot\left|\frac{d\varphi(\varepsilon_{0e})}{d\varepsilon_{0e}}\right|, \tag{8}$$

where: $\varphi(\varepsilon_{0e})=(a-b)/(2\cdot\Lambda^2)$, $d\varphi/d\varepsilon_{0e}=(1-a/b)/(2\cdot\Lambda^2)$, $a=a(\varepsilon_{0e};\Lambda)=\varepsilon_{0e}+\Lambda^2+1$,

$b=b(\varepsilon_{0e};\Lambda)=\varepsilon_{0e}^2+2\cdot\varepsilon_{0e}\cdot(1+\Lambda^2)+(1-\Lambda^2)^2$.
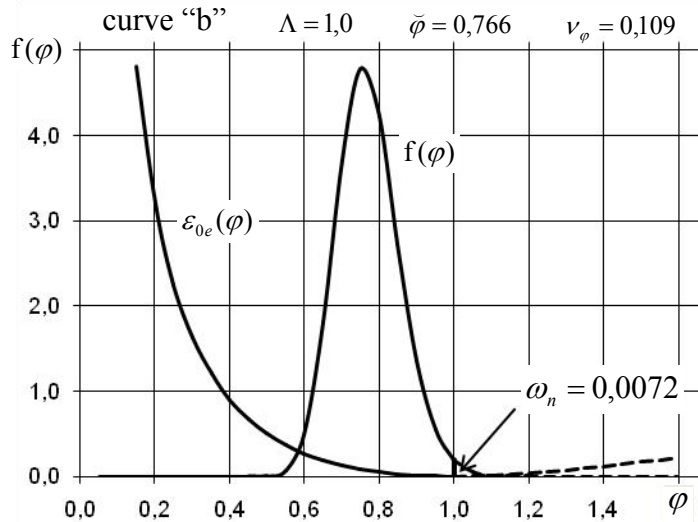

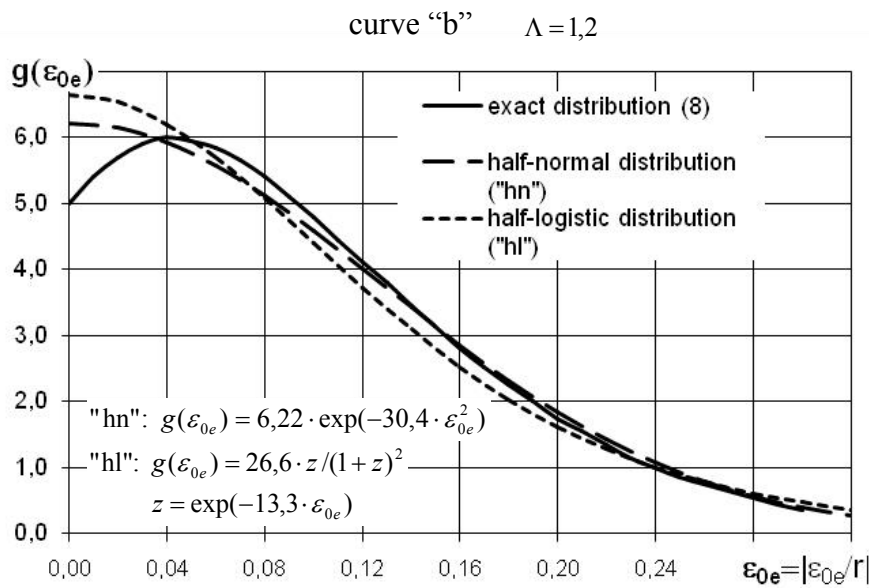Figure 4(a). The Example of $\varepsilon_{0e}(\varphi)$ and $f(\varphi)$ Relationship

Figure 4(b). The Example of Probability Density Function $g(\varepsilon_{0e})$

Example results of calculation according to Eq. 8, for bucking curve "b" and $\Lambda=1,2$, were shown in Figure 4(b). Density of "exact" distribution ("8") according to Eq. 8 shows (beside of close surroundings of $\varepsilon_{0e}=0$ point) very good compatibility with density of half-normal distribution ("hn") and good compatibility with density of half-logistic distribution ("hl"). One-parameter half distributions mentioned above were matched according to mean values conformity criterion: $\overline{X}_e=\overline{X}_{hn}=\overline{X}_{hl}$ (where $\overline{X}\equiv\overline{\varepsilon_{0e}}$).

Mean values $\bar{\varepsilon}_{0e}$ and standard deviations $\mu_{\varepsilon 0e}$, determined from numerical integration of Eq. 8, for appropriate half-normal distributions $\underline{\varepsilon}_{0e}$, are related to Λ almost linearly (Figure 5(a))

$$\bar{\varepsilon}_{0e} = C_{\bar{\varepsilon}} \cdot \Lambda, \qquad \mu_{\varepsilon 0e} = C_{\mu\varepsilon} \cdot \Lambda, \tag{9}$$

with direction coefficients $C_{\bar{\varepsilon}}$ and $C_{\mu\varepsilon}$ given in Table 3.

Value of coefficient $C_{\mu\varepsilon}^*$ (for relationship $\mu_{\varepsilon 0e}^* = C_{\mu\varepsilon}^* \cdot \Lambda$) corresponding to normal distribution $\underline{\varepsilon}_{0e}^*$ with changeable signs and mean value $\bar{\varepsilon}_{0e}^* = 0$ is obtained (Table 3) from relationship $C_{\mu\varepsilon}^* = C_{\mu\varepsilon} / \sqrt{1 - 2/\pi}$ (Machowski [3]).

In Figure 5(b) values of $\varepsilon_{0e}(\Lambda)$, obtained from half-normal distribution $\underline{\varepsilon}_{0e}$ with parameters according to Table 3, were compared, for bucking curve "b", with values from Standard Recommendations and values from formula (6). Straight lines "1" and "2" are obtained for assumed probability ω of exceeding ε_{0e} value (top quantiles) in half-normal distribution. Straight line "2" corresponding to value $\omega = 2\%$ turns out very close to straight line "3" characterized by equation $\varepsilon_{0z} = 0,3 \cdot \lambda / 100 = 0,3 \cdot \Lambda \cdot \lambda_1 / 100$ (for $\lambda_1 = 0,84$) – representing traditional British Recommendations (BS 449). Broken line "4", according to Eurocode 3 – with equation: $\varepsilon_{0z} = 0,34 \cdot (\bar{\lambda} - 0,2)$ - for $\bar{\lambda} > 0,2$ and $\varepsilon_{0z} = 0$ - for $\bar{\lambda} \le 0,2$, (taking relationship $\Lambda = 1,12 \cdot \bar{\lambda}$ into consideration) shows good compatibility with curve "5" obtained from (6) substituting $\chi(\bar{\lambda})$ in place of $\varphi(\lambda)$ and $\bar{\lambda}$ in place of Λ.
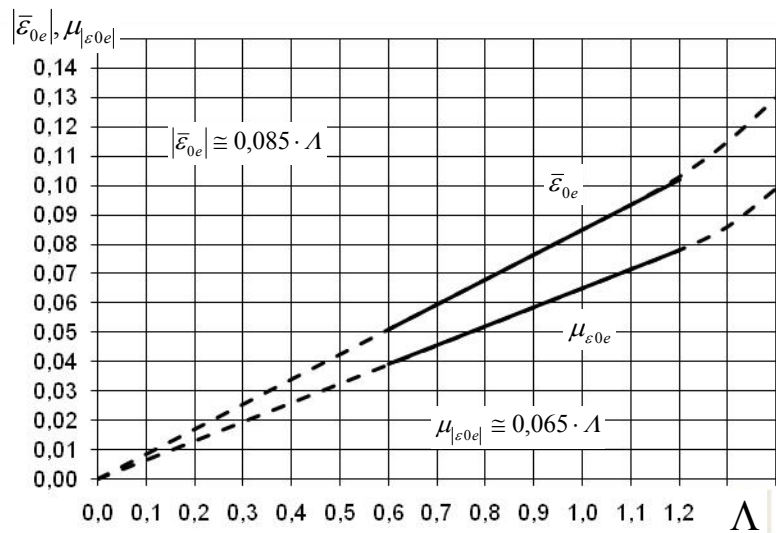

Figure 5(a). Examples of Relation $\bar{\varepsilon}_{0e}(\Lambda)$ and $\mu_{\varepsilon 0e}(\Lambda)$ for Curve "b"
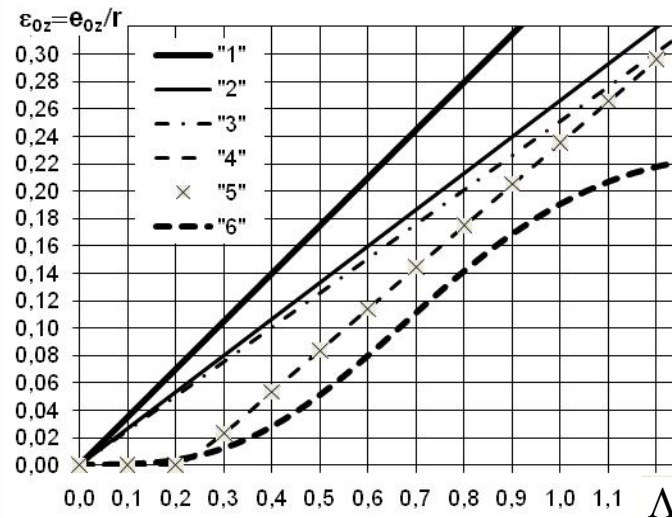
Figure 5(b). Comparison of relation $\varepsilon_{0e}(\Lambda)$ according to different formulas
("1" – random for $\omega = 1{,}35‰$, "2" – random for $\omega = 2\%$, "3" – "$0{,}3\lambda/100$", "4" – "$0{,}34(\bar{\lambda} - 0{,}2)$",
"5" – acc. to Eq. 6 for $\bar{\lambda}$ and $\chi(\bar{\lambda})$, "6" – acc. to Eq. 6 for Λ and $\varphi(\Lambda)$

Table 3. Coefficients values for formula (9)

buckling curve	$C_{\bar{\varepsilon}}$	$C_{\mu\varepsilon}$	$C^*_{\mu\varepsilon}$
a	0,065	0,045	0,075
b	0,085	0,065	0,110
c	0,120	0,085	0,140

Occurrence of φ and Λ quantities in non-linear form in Eq. (6) cause significant mutual discrepancy between curves "5" and "6" (Figure 5(b)) despite of affirmed earlier good compatibility of buckling curves (Figure 3).

3.   RANDOM EQUIVALENT INITIAL TILT OF FRAME

Mathematical model of column single story initial tilt was determined on the basis of column out-of-plumbs post-fabrication measurements, carried out after all frames erection and after construction of all floors.

Most extensive statistical analysis of measurements mentioned above was conducted in (Machowski [3, 12]) which also includes results obtained earlier by Beaulieu (Beaulieu and Adams [13]) and Lindner (Lindner and Gietzelt [14]).

Conducted analysis showed that that mathematical model of stationary gaussian random noise $\underline{\phi}^x_{ijk}$ and $\underline{\phi}^y_{ijk}$ (stationary random series with mean value $\bar{\phi} = 0$ and constant variance $D_\phi = \mu^2_\phi = \text{const.}$) is justified if empirical variance fulfils a constraint

$$\mu^2_\phi \le 3\,(‰)^2, \tag{10}$$

what agrees with keeping initial tilt standard tolerance.

The second conclusion was that only exist weak autocorrelation dependence between tilts of columns in the same vertical planar frames and lack of correlation between any other initial tilts.

For design purposes it is very convenient to assume one random value of equivalent initial tilt for frame as a whole $\underline{\phi}^{EFF}$ instead of column initial tilts random sequences $\underline{\phi}_{ip}$.

Post-fabrication column out-of-plumbs cause additional bending moments from vertical load for frame as vertical cantilever (Machowski, A. [3, 12]).

For bar-disk analytical scheme of multistory skeletal structure with rigid floor-disks effective initial random tilt for i-th story of building $\underline{\phi}_i^{eff}$ may follow from conservation of global moment increment condition (if torsional effect for building as vertical cantilever is neglected)

$$\Delta \underline{M}_i^{\phi} = \sum_{p=1}^{s} P_{ip} \cdot h_i \cdot \underline{\phi}_{ip} = P_i \cdot h_i \cdot \underline{\phi}_i^{eff} , \tag{11}$$

where: $P_i = \Sigma P_{ip}$, $(p = 1\dots s.)$ - sum of all vertical loads acting on building above i-th story,
P_{ip} (for s columns $i = 1, 2,\dots, s.$ on i-th story of building) – sum of vertical loads above i-th story in p-th column,

hence i-th story equivalent initial tilt

$$\underline{\phi}_i^{eff} = \sum_{p=1}^{s} w_{ip} \cdot \underline{\phi}_{ip} = \mathbf{w}_i \, \underline{\phi}_i^{T} , \tag{12}$$

Story random initial tilt $\underline{\phi}_i^{eff}$ is normal random variable with parameters (Machowski [3, 12]):

$$E\left\{\underline{\phi}_i^{eff}\right\} = 0, \quad \mu_{\phi i}^2 = k_{c,i}^2 \cdot \mu_{\phi}^2 , \tag{13}$$

where

$$k_{c,i}^2 = \mathbf{w}_i \boldsymbol{\rho}_s \mathbf{w}_i^{T} = \sum_{p=1}^{s} w_{ip} \cdot \sum_{q=1}^{s} w_{iq} \cdot \rho_{pq} \tag{14}$$

is positively defined quadratic form of s-variables: $w_{i1},\dots,w_{ip},\dots w_{is}$. with symmetric matrix of coefficients $\boldsymbol{\rho}_s$ equal to normalized correlation matrix $\boldsymbol{\rho}_s$ of random vector $\underline{\phi}_i$.

Values of reduction coefficient $k_{c,i}$ according to Eq. 14 have been analysed in detail in (Machowski [3, 12]). Conducted analysis showed that among standard formulas closest to obtained result is that in Polish Standard [6], on condition that only columns with vertical load (above i-th story) arrangement parameter $c \geq 0,5$ are taken into account.

Safe approximation of effective random initial tilt for frame as a whole may be defined as follows

$$\underline{\phi}^{EFF} = \max_{i=1}^{n} \left| \underline{\phi}_i^{EFF} \right| = \max_{i=1}^{n} \left| \sum_{t=i}^{n} V_t \cdot \sum_{q=i}^{t} h_q \cdot \underline{\phi}_q^{eff} \cdot \left(\sum_{t=i}^{n} V_t \cdot \sum_{q=i}^{t} h_q \right)^{-1} \right|, \tag{15}$$

$\underline{\phi}_i^{EFF}$ – effective random initial tilt for frame as a whole, which guarantee safe estimation of additional bending moment for i-th story of frame as vertical cantilever,

$\underline{\phi}_i^{eff}$ – according to Eq. 12,

V_t – sum of vertical loads imposed immediately to t-th story.

Analyses conducted in (Machowski [3, 12]) showed that within confines of discussed conception reduction of initial tilt standard deviation and characteristic value depending on story number is unfounded. According to extensive analyses presented in (Rondal and Maquoi [8], Machowski and Tylek [15]) this reduction is justified only in special cases, e.g. with reference to frames fulfilled "strong columns" condition (columns remain elastic up to plastic mechanism formation).

4.   JOINT EFFECT OF EQUIVALENT INITIAL TILT AND INITIAL BOW

Statistically based models of equivalent imperfections $\underline{e}_{0e}$ and $\underline{\phi}_{0e}$, according to chapters 2 and 3, first of all may be used to verify Standard conceptions of steel skeletons calculation. This verification may apply, among others things, to often criticized effective length conception for sway frames and described in p. 6.3.4 Eurocode 3 [5] so called "general method" depending on reduction of resistance coefficient $\alpha_{ult,k}$ by means of factor χ_{op} determined as Standard flexural buckling coefficient χ or Standard lateral-torsional buckling coefficient χ_{LT} - calculated for "global non-dimensional slenderness" $\overline{\lambda}_{op}$, connected with out-of-plane buckling of a structural component. Analysis of Standard conceptions mentioned above with application of proposed models of $\underline{e}_{0e}$ and $\underline{\phi}_{0e}$ would require, as it seems, separate extensive study.

Another important problem that will be consider farther in this article, is influence of both random equivalent imperfections on total imperfections effect. In this case random variability of $\underline{e}_{0e}$ sign (direction) in column assembly elements may be important. Taking into account of this last effect requires, even in the simplest cases, to consider examples of multistory steel frames.

Joint effect of random equivalent initial tilt $\underline{\phi}_{0e}$ and random equivalent initial bow $\underline{e}_{0e}$ in "advanced analysis" was considered on the example of 5-story steel skeleton (Figure 6). Vertical loads from floors, roof and walls of the building are carried by floor beams on five transversal rigid frames located in axes 1-1 to 5-5 of building horizontal projection. Skeleton bracing system, carrying horizontal load, is made up, among transversal frames mentioned above, three equal two-bay rigid frames located in axes: A-A, B-B and C-C (see horizontal projection in Figure 6). Skeleton filling consist of floors and flat roof with reinforced concrete supporting structure, (rigid in own plane and nonflexibly connected with beams) and light-weight partition and curtain walls. It should be noticed that plane of every longitudinal frame agrees with column minor stiffness plane (Figures 6 and 7).
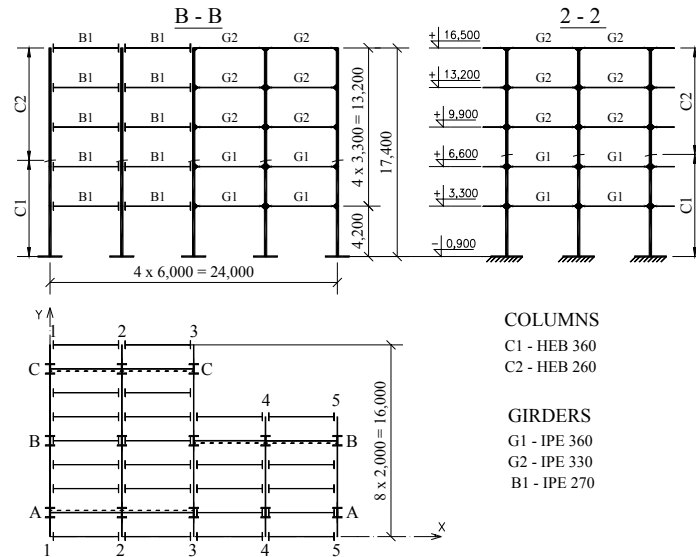
Figure 6. Analysed Skeletal Framed Steel Structure

Considering vertical planar frame of longitudinal bracing system (e.g. C-C) acc. to Figure 6 and neglecting torsional effects for building as vertical cantilever substitute static system of planar frame (Figure 7) was assumed. This system was loaded by realistic vertical loads in the form of concentrated forces Q_{11}^C to Q_{n3}^C – putted in nodes and fictitious imperfectional load uniformly distributed on columns: $q_{11} ... q_{n3}$ (as in [5]) – balanced by reactions $R_{11} ... R_{n3}$.

Influence of column initial tilts of skeleton braced in longitudinal direction by three identical frames, joined by rigid floor disks, was taken into consideration by adding to planar frame fictitious system (Figure 7) consisted of bars ideally rigid, connected by hinges with each other and with frame. To the nodes of system mentioned above following loads were applied: vertical loads $V_1 ...$ $V_i ... V_n$ equal to 1/3 of sum of Q_i vertical loads on i-th skeleton floor and couples of forces $P_i\phi_{0i}$ ($i = 1, 2, ..., n$.) representing equivalent imperfectional load from initial tilts.
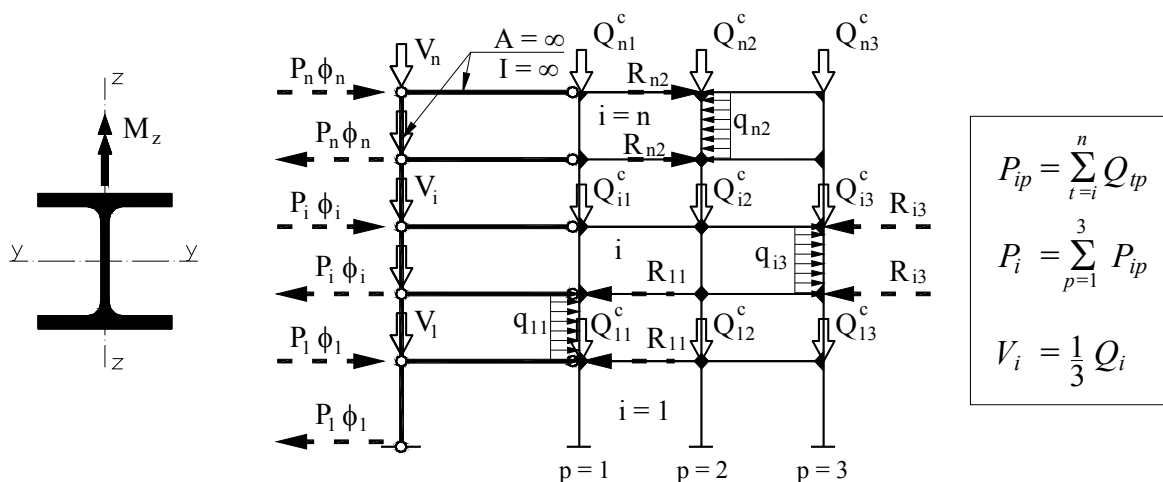

Figure 7. Substitute Static System of Analyzed Planar Bracing System of
5-story Skeletal Steel Structure (Q_{ip} – Total Vertical Load of Building as a Whole i-th story)

Random sequences of story initial tilts were computer generated in the form of vector $\underline{\phi}^{eff} = \{\underline{\phi}_i^{eff}\}$ which elements were normal variable with parameters according to Eq. 13. Week correlation between initial tilts in vertical sequences was neglected.

Mathematical model of column random equivalent initial bow was product of random initial bow and random binary sequence (with elements 1 and -1). Value of column random initial bow was determined on the basis of knowledge of probability density function and characteristics of random dimensionless column bow distribution (according to p.2). Normal distribution with parameters $\{\bar{\varepsilon}_{0e}^* = 0, \ \mu_{\varepsilon 0e}^* = C_{\mu\varepsilon}^* \cdot \Lambda\}$ ($C_{\mu\varepsilon}^*$ according to Table 3) was assumed. It was also assumed that column splices are located on every story (above bottom node of column) so there is no correlation between initial bows of individual columns.

Additional effect of column equivalent initial bows on frame carrying capacity (associated with limit point on frame equilibrium path) was determined by comparison of frame initial tilt $\underline{\phi}^{EFF}(\underline{\phi}_{0e})$ (substitutes for random sequence of story initial tilts only – Figure 8a) standard deviation with frame initial tilt $\underline{\phi}^{EFF}(\underline{\phi}_{0e}, \underline{e}_{0e})$ (substitutes for story random initial tilts and column random initial bows – Figure 8b) standard deviation values. In both cases the same sequences of story random initial tilts were considered.
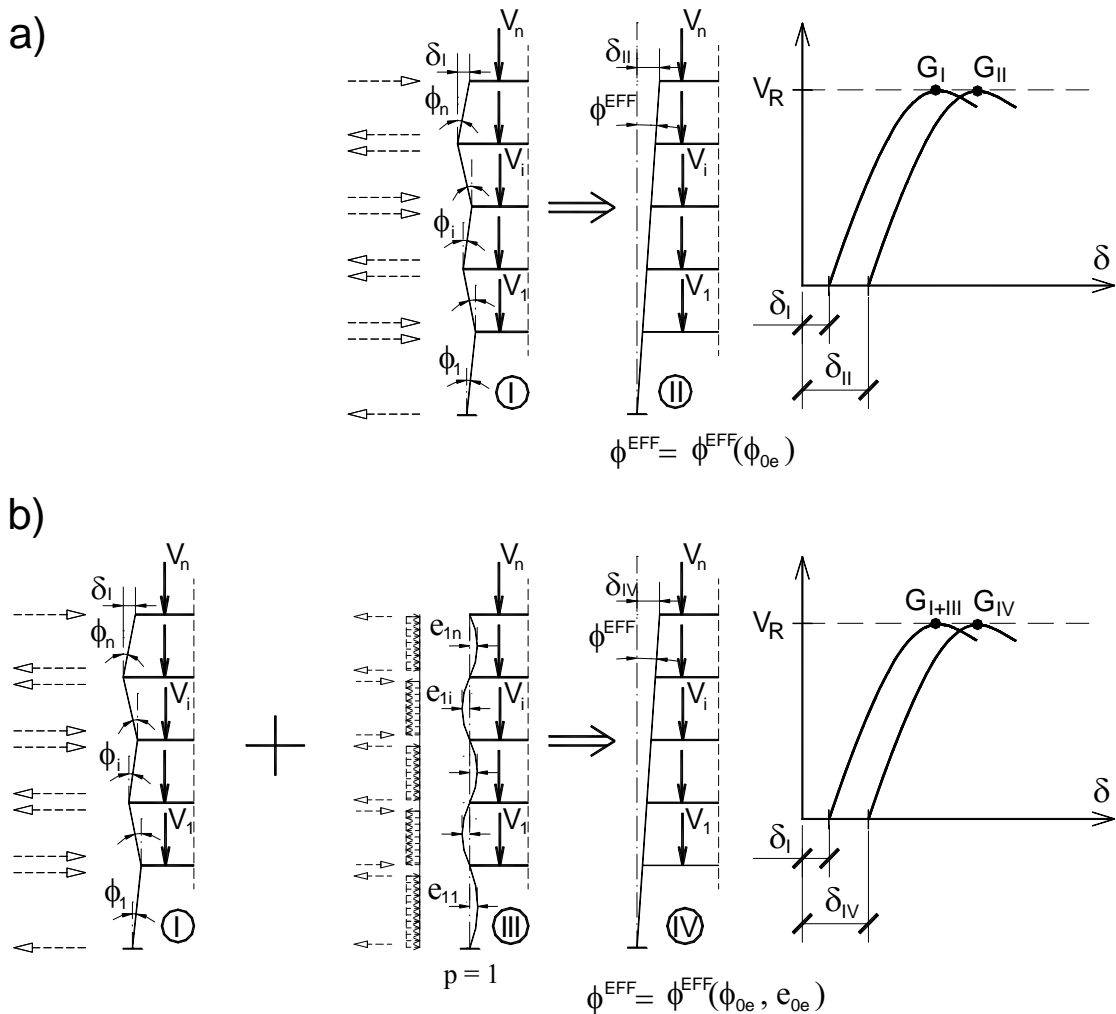

Figure 8. Random Sequence of Story Initial Tilts, Random Set of Column $p = 1$ Initial Bows and Its Equivalent Forces; Equivalent Tilts of Frame as a Whole and Corresponding Paths of Equilibrium

According to applied simulation procedure, for every realization of equivalent imperfectional loads set (Figure 7) respective frame equilibrium path and frame carrying capacity were determined. Next the effective initial tilt of frame as a whole ϕ^{EFF} was chosen in agreement with condition of frame limit carrying capacity conservation (Figure 8). Equivalent random initial tilt of plane frame as a whole $\underline{\phi}^{EFF}$ was determined on the basis of conservation of carrying capacity associated with limit point on frame equilibrium path criterion. Calculations were conducted for 700 elements population.

In order to obtain frame equilibrium path and frame limit carrying capacities computer program ANSYS, based Finite Element Method, were utilized. Two-dimensional bar structure model with regular mesh and elastic-plastic (bilinear) model of material was assumed. Description of the material model was based on Huber-Mises-Hencky plasticity criterion, associative flow rule and rule of kinematic hardening. Development of plastic zones (in cross section and along length of element) and large displacements (translations and rotations) with small deflections were take into consideration.

Difference between standard deviations of frame initial tilt $\underline{\phi}^{EFF}(\underline{\phi}_{0e})$ and frame initial tilt $\underline{\phi}^{EFF}(\underline{\phi}_{0e}, \underline{e}_{0e})$ obtained from conducted analysis is lower than 2% and indicates that additional influence of column random equivalent initial bows on frame carrying capacity in advanced analysis may be neglected.

Results of earlier works (De Luca and Mele [17]) indicated that interaction of global (tilts) and local (bows) geometric imperfections causes reduction of frame carrying capacity by 10%, but authors [17] assumed deterministic (instead of random) values of equivalent imperfections and selected some combinations of global and local equivalent geometric imperfections, compatible with first buckling eigenvector of ideal elastic frame and combinations of initial bows acceptable for the sake of columns splices (Figure 9).
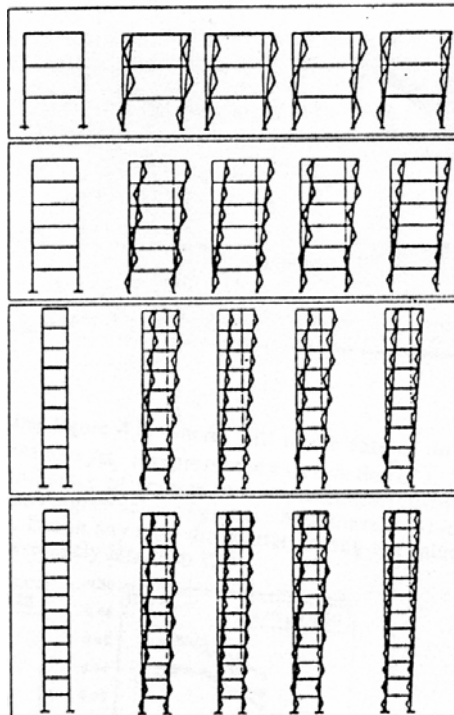

Figure 9. Set of Local and Global Geometrical Imperfections Combination Analyzed in [17]

5.   CONCLUSIONS

Verification of Standard recommendations of steel skeletons design with equivalent geometrical imperfections (column initial tilt ϕ_0 and bow e_0) should base on probabilistic models of these imperfections and takes into account its interaction. Application of random models and imperfections acting together should lead to taking into consideration of favourable effects – similar to these which we deal with in case of random load combinations.

Possibility of applying approach mentioned above offers this work model of equivalent random initial bow of compressed bar $\underline{e}_0$. It is obtained out of randomization of buckling coefficient in well-known deterministic formula of equivalent initial bow. This model together with known from earlier works, e.g. authors' works [3, 12, 15, 16], model of equivalent random initial tilt $\underline{\phi}_0$, allows analyses of mentioned above Standard reccomendations.

In the paper effects of column initial tilts and initial bows interaction were investigated using probabilistic approach, introducing into calculations, in elastic-plastic structure behaviour, statistically based models of equivalent imperfections.

Analysis of 2-bay 5-story frame planar bracing system with random sequences of story initial tilts and random sets of column initial bows showed slight influence of column random initial bows on frame carrying capacity and equivalent initial tilt of frame as a whole $\underline{\phi}^{EFF}$. Influence of interaction of global and local imperfections on frame carrying capacity was lower than 2%.

Results of conducted analysis justify passing over of local geometric imperfections influence in planar frames advanced analysis. It also shows that Eurocode 3 procedure of steel frame design, recommending to introduce in stage on static calculations only frame equivalent initial tilt while influence of column equivalent initial bows is taking into account in beam-column design formulas.

REFERENCES

[1]   Chen, W.F. and Toma, S., "Advanced Analysis of Steel Frames", London-Tokyo: CRC Press, 1994.
[2]   Narayanan, R. ed, "Steel Framed Structures, Stability and Strength", Elsevier Science, 1985.
[3]   Machowski, A., "Problems of Limit States and Reliability of Steel Multistory Building Frames", Monograph No. 262, Cracow University of Technology, 1999 [in Polish].
[4]   Fukumoto, Y. and Itoh, Y., "Multiple Buckling Curves Based on Experimental Data", Construction Métállique, 1984, Vol. 3 [in French].
[5]   CEN "EN 1993-1-1. Eurocode 3, Design of Steel Structures, Part 1.1: General Rules and Rules for Buildings".
[6]   PKNMiJ, "PN-90/B-03200, Steel Structures, Design Rules" [in Polish].

[7]   Allen, D., "Merchant-Rankine Approach to Member Stability", Journal of the Structural Division, 1978, 104 (ST.12), pp. 1909-1914.

[8]   Rondal, J. and Maquoi, R., "The Ayrton-Perry Formulation for Buckling of Metallic Bars", Construction Metállique, 1979, 4, pp. 41-53 [in French].

[9]   Murzewski, J., "Design of Steel Structures for Differentiated Reliability Levels", Archives of Civil Engineering, 2008, LIV(1), pp. 209-237.

[10]   ECCS, "European Specifications for Steel Structures", 1-st ed; 1974.

[11]   Papoulis, A., "Probability, Random Variables and Stochastic Processes", McGraw-Hill Inc, 1965.

[12]   Machowski, A., "Initial Random Out-of-plumbs of Steel Frame Columns", Archives of Civil Engineering, 2002, XLVIII(2), pp. 207-226.

[13]   Beaulieu, D. and Adams, P.F., "The Results of a Survey on Structural Out-of-plumbs", Canadian Journal of Civil Engineering, 1978, Vol. 5, pp. 642-470.

[14]   Lindner, J. and Gietzelt, R., "Evaluation of Imperfections of Support – Elements", Stahlbau, 1984, Vol. 4, pp. 97-98 [in German].

[15]   Machowski, A. and Tylek, I., "Conceptions of Equivalent Imperfections in Analysis of Steel Frames", The International Journal of Advanced Steel Construction, 2008, Vol. 4, No. 1, pp. 13-25.

[16]   Tylek, I., "Equivalent Geometrical Imperfections of Multistory Steel Building Frames", Doctoral Thesis, Cracow University of Technology, 2007 [in Polish].

[17]   De Luca A. and Mele, E., "Analysis of Steel Frames in the Light of Eurocode 3 and New Research Results", In: White, D.W. and Chen, W.F. ed., "Plastic Hinge Based Methods for Advanced Analysis and Design of Steel Frames", SSRC, Lehigh Univ., 1993, pp. 97-152.